

Active Disturbance Rejection Control for Robot Manipulator

Carlos E. Martínez-Ochoa¹, Ivón O. Benítez-González², Ariel O. Cepero-Díaz³, José R. Nuñez-Alvarez^{4,*},
Carlos G. Miguélez-Machado⁵, Yolanda E. Llosas-Albuerne⁶

¹ Integral Automation Company CEDAI, Santiago, of Cuba, Cuba

^{2,5} Technological University of Havana “José Antonio Hecheverría,” CUJAE, Havana, Cuba

³ Cuban Enterprise for Airports Services, ECASA, Havana, Cuba

⁴ Energy Department, Universidad de la Costa, Colombia

⁶ Department of Electricity, Technical University of Manabí, Ecuador

Email: ¹ CarlosMO@cedai.com.cu, ² novi@automatica.cujae.edu.cu, ³ ariel.cepero@hav.ecasa.avianet.cu,

⁴ jnunez22@cuc.edu.co, ⁵ cmiguelzmachado@gmail.com, ⁶ yolanda.llosas@utm.edu.ec

*Corresponding Author

Abstract—Active Disturbance Rejection Control (ADRC) is a control methodology used in chemical processes, aircraft, motors, and other systems. This paper compares the results of an ADRC controller to a Proportional Integral Derivative controller (PID), applied to two degrees of freedom robots. A Linear Extended State Observer (LESO) is used to reconstruct the state variables and unknown parameters needed to control the position of each link. The ADRC can achieve the tracking position and estimate the velocity of each link. The results of the simulation program are shown.

Keywords—ADRC; Control; Disturbance; Observer; Robot.

I. INTRODUCTION

Robot manipulators have been taking significant parts in the industry: welding [1], the surgery field, and many other critical operations. Therefore, performance criteria such as low energy consumption and faster process have risen correspondingly. The lightweight structure of flexible link manipulators brings advantages over conventional, bulky rigid manipulators [2]. Many factors must be carefully considered when designing a robot arm, such as the geometry and size of the required workspace and the environmental conditions of its workspace. Of these factors, the most challenging one is the inverse kinematics that relates the desired motion and orientation of the end-effector to its joint displacements [3], [4].

The demands of lightweight robotic systems and space applications have stimulated the study of flexible link manipulators. However, they suffer from undesired vibrations caused by the commanded motions. The detrimental effects degrade positioning accuracy, capable operating speeds, workspace size, and reliability. Therefore, there is a need to control unwanted oscillations and inflexible link manipulators [5].

Although the robot ontology parameters are fixed, the changing load and uncertain disturbances can affect the robustness of the control and introduce significant mechanical vibrations. Moreover, the control systems during high-speed motion are challenged mainly by the severe multi-joint torque coupling, large inertia changes, and significant nonlinear effects. The stable movement variation refers to the

robot maintaining a smooth, non-jitter throughout the movement. The stability must be determined by the actual requirements, such as in the blade grinding process, where the trajectory error must be less than 0.05 mm [6].

A dynamic feedback control design is developed for robotic manipulators' trajectory tracking control problems with flexible joints. In this control design, the position measurements of the link and motor are needed, such that a reduced-order observer is used to estimate the required velocities for control [7].

The conventional observer assumes that an exact mathematical model is available. However, the physical motion control systems usually contain multiple uncertainties, such as unknown nonlinear friction and load disturbance, to name a few. Therefore, the fundamental challenge in practice is to make the Proportional Derivative control-based observer capable of dealing with uncertainties far beyond the known model information in motion processes [8].

Most of the existing methods proposed disturbance attenuation techniques to solve this problem. Less-known solutions are proposed to estimate and cancel the disturbance directly. Many disturbance estimators have been presented in the literature, such as disturbance observer, unknown input observer, disturbance observer, and extended state observer (ESO) [9], [10]. Based on the ESO, a new algorithm called “Active Disturbance Rejection Control” (ADRC) has been developed [8], [9], [10]. This control strategy's main idea is to estimate and compensate for unknown dynamics and disturbances actively. In addition, it requires very little information about the plant. Then the controller uses the information from the ESO to control the system instead of being dependent on the mathematical model [11].

Professor Jingqing Han proposed the ADRC control method in the 1980s. It does not need to know the exact model of the system. The extended state observer of this controller estimates the system's “total disturbance” and then compensates for such disturbance [12], [13], [14], [15]. The ADRC is not based on plant model analysis because system behaviors could change unexpectedly, and the plant models



may become unreliable. As an emerging approach, ADRC uses a controller-observer pair to treat external and internal disturbances and uses plant parameter variations or uncertainties as an element, not to be modeled analytically but to be rejected as a generalized “total disturbance.” The control signal responds directly to cancel the “total disturbance,” thus making the controller design almost model-free [16].

This document's contribution is comparing the performance of three different controllers, an ADRC, an ADRC+FC, an ADRC with torque friction compensation, and a Proportional Integral Derivative (PID) controller, for controlling a two-degree-of-freedom robot. This robot belongs to an investigation laboratory. The velocity of the robot links is estimated internally using the ADRCs. Thus, costs are reduced because mechanical devices are not used to measure speed. The results are statistically analyzed.

The paper is organized as follows: Description of the robot is made in Section 2; Control of the robot is presented in Section 3; Control diagrams and trajectories planning, in Section 4; and Simulation results in Section 5. Finally, they have shown the Conclusion, Future works, and References.

II. ROBOT DESCRIPTION

This robot belongs to the Robotics Laboratory from the CICESE Research Center, Mexico. It has two rigid links of lengths l_1 (shoulder) and l_2 (elbow) and masses m_1 and m_2 , respectively. This robot moves on the plane x - y , as illustrated in Fig. 1 [17].

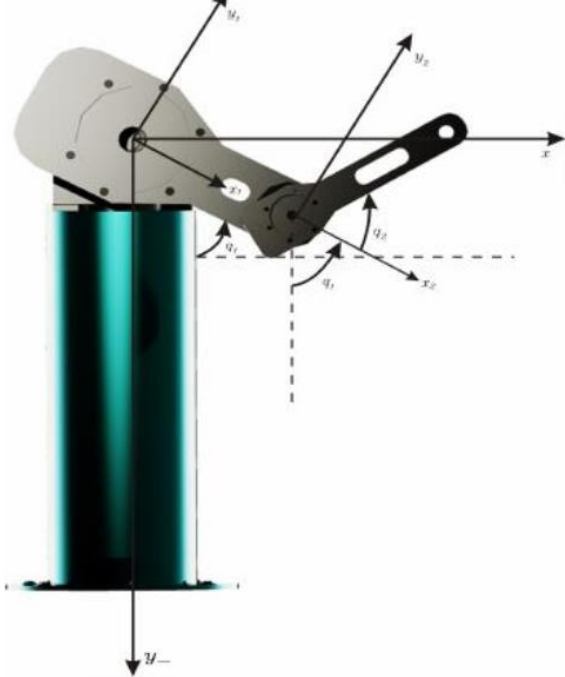


Fig. 1. Two degrees direct-drive robot manipulator [17].

The degrees of freedom are associated with the angle q_1 , measured from the vertical position, and q_2 , measured relative to the extension of the first link toward the second link, both being positive counter clockwise [17], [18].

A. Direct Kinematics Model

The direct kinematic model is given by (1) [19], [20].

$$\begin{aligned} x &= l_1 \sin(q_1) + l_2 \sin(q_1 + q_2) \\ y &= -l_1 \cos(q_1) - l_2 \cos(q_1 + q_2) \end{aligned} \quad (1)$$

B. Inverse Kinematics Model

The inverse kinematic model allows us to obtain the joint positions q in terms of the position and orientation of the end-effector. The last link referred to the base reference frame. The desired common positions q_d is obtained from trigonometric manipulations as (2) [19], [20].

$$\begin{aligned} q_{d1} &= \tan^{-1} \left(\frac{x_d}{-y_d} \right) - \tan^{-1} \left(\frac{l_2 \sin(q_{d2})}{l_1 + l_2 \cos(q_{d2})} \right) \\ q_{d2} &= \cos^{-1} \left(\frac{x_d^2 + y_d^2 - l_1^2 - l_2^2}{2l_1 l_2} \right) \end{aligned} \quad (2)$$

C. Robot's Dynamic Model

The dynamic equations that model the robot arm are obtained by applying Lagrange's in (3) [6], [17], [18], [19], [20], [21], [22], [23], [24], [25].

$$\frac{d}{dt} \left[\frac{\partial L}{\partial \dot{q}_i} \right] - \frac{\partial L}{\partial q_i} = \tau_i, \quad i = 1, 2 \quad (3)$$

For control purposes, in the compact form in (4)-(8) [17], [18], [26] as

$$\begin{bmatrix} M_{11}(q) & M_{12}(q) \\ M_{21}(q) & M_{22}(q) \end{bmatrix} \ddot{q} + \begin{bmatrix} C_{11}(q, \dot{q}) & C_{12}(q, \dot{q}) \\ C_{21}(q, \dot{q}) & C_{22}(q, \dot{q}) \end{bmatrix} \dot{q} + \begin{bmatrix} g_1(q) \\ g_2(q) \end{bmatrix} + \begin{bmatrix} f_1(\dot{q}) \\ f_2(\dot{q}) \end{bmatrix} = \tau \quad (4)$$

$$M_{11}(q) = m_1 l_{c1}^2 + m_2 [l_1^2 + l_2^2 + 2l_1 l_{c2} \cos(q_2)] + I_1 + I_2$$

$$M_{12}(q) = m_2 [l_{c2}^2 + l_1 l_{c2} \cos(q_2)] + I_2 \quad (5)$$

$$M_{21}(q) = m_2 [l_{c2}^2 + l_1 l_{c2} \cos(q_2)] + I_2$$

$$M_{22}(q) = m_2 l_{c2}^2 + I_2$$

$$C_{11}(q, \dot{q}) = -m_2 l_1 l_{c2} \sin(q_2) \dot{q}_2$$

$$C_{12}(q, \dot{q}) = -m_2 l_1 l_{c2} \sin(q_2) [\dot{q}_1 + \dot{q}_2] \quad (6)$$

$$C_{21}(q, \dot{q}) = m_2 l_1 l_{c2} \sin(q_2) \dot{q}_1$$

$$C_{22}(q, \dot{q}) = 0$$

$$g_1(q) = (m_1 l_{c1} + m_2 l_1) g \sin(q_1) + m_2 l_{c2} g \sin(q_1 + q_2) \quad (7)$$

$$g_2(q) = m_2 l_{c2} g \sin(q_1 + q_2)$$

$$f_1(\dot{q}) = b_1 \dot{q}_1 + f_{c1} \operatorname{sgn}(\dot{q}_1) \quad (8)$$

$$f_2(\dot{q}) = b_1 b_2 \dot{q}_2 + f_{c2} \operatorname{sgn}(\dot{q}_2)$$

Where $M(q)$ is inertia matrix that is symmetric positive definite and has dimension $n \times n$. Its elements are functions only of q . $C(q, \dot{q})$ is matrix of centrifugal and Coriolis forces, order $n \times n$, and its elements are functions of q and \dot{q} . $g(q)$ is vector of dimension n of gravitational forces. $f(\dot{q})$ is Coulomb and viscous frictions have been considered to

model the friction torque. τ is vector of dimension n called the vector of external forces, in general, corresponds to the torques and forces applied by the actuators at the joints. g is gravity acceleration.

Physical parameters of robot arm: $l_1 = l_2 = 0.45$ m, $l_{c1} = 0.091$ m, $l_{c2} = 0.048$ m; $m_1 = 23.902$ kg, $m_2 = 1.285$ kg, $I_1 = 1.266$ kg m², $I_2 = 0.093$ kg m² and $g = 9.81$ m/s². Where, f_{c1} , f_{c2} and b_1 , b_2 represent coefficients of Coulomb and viscous frictions for the shoulder and elbow joints, respectively. From experimental tests they were obtained the following numerical values of these coefficients: $b_1 = 2.288$ Nms, $b_2 = 0.175$ Nms, $f_{c1} = 7.17$ Nm for $\dot{q}_1 > 0$, $f_{c1} = -8.049$ Nm for $\dot{q}_1 < 0$ and $f_{c2} = 1.734$ Nm [17], [18].

In controlling robot manipulators, disturbances may come from unmodeled dynamics or additive sensor noise, which are common in practice. Consequently, in the case where the parametric uncertainty comes from the mass or the inertia corresponding to the object (load) manipulated by the robot, the manipulated object may be considered part of the robot's last link [19].

A robot drive train comprises an actuator or motor and transmission to connect it to the link. A common approach to robot joint control is to consider each joint or axis as an independent control system that attempts to follow its joint angle trajectory accurately. These turns are complicated due to various disturbance torques produced by the gravitational force, velocity and acceleration coupling, and friction that acts on the joint [27].

III. ROBOT CONTROL

The control of robot manipulators in joint space is the most available in the literature on robot control [19]. The classical PID controller implements the basic principle in error-based feedback control, as shown in Fig. 2, where the error between the setpoint r and process output y is given by $e = u - y$. The controller is (9) [9], [19], [28], [29], [30], [31], [32] as

$$u = K_d \frac{de}{dt} + K_p e + K_i \int_0^t e dt \quad (9)$$

where K_d , K_p , and K_i , are the derivative, proportional, and integral gains, respectively.

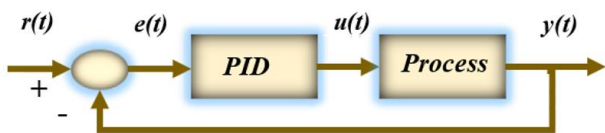


Fig. 2. Control loop structure of PID for the process

The usefulness of the PID controller lies in its general applicability to most control systems. In the field of process control systems, the basic and modified PID control schemes have proved their usefulness in providing satisfactory control, despite the that in many given situations, they may not offer optimal control [29].

The integral model, viewed in isolation: its pole at the origin, is detrimental to loop stability. It also gives rise to the

undesirable effect (an actuator saturation) known as a wind-up [28].

The main limitation of the derivative mode, viewed in isolation, is its tendency to yield large control signals in response to high-frequency control errors, such as errors induced by setpoint changes or measurement noise [28], [29], [30], [31], [32].

A. Disturbance Rejection Control Algorithm Used

The ADRC is based on an extension of the system model with an additional and fictitious state variable, representing those elements of the system dynamics that the user does not include in the mathematical description of the plant. These virtual states (sum of internal and external disturbances, sometimes denoted as a total disturbance) are estimated online and used in the control loop to decouple the system from the actual perturbation acting on the plant (10) [34], [35], [36], [37], [38], [39] as

$$\dot{y}(t) = f(y(t), \dot{y}(t), \ddot{y}(t), \dots, y^{(n)}(t)) + d(t) + bu(t) \quad (10)$$

Where d is the external disturbance, u is the input, y is the output, and b is a real constant of the system that is known indirectly through the estimated b_0 . The expression $f(y(t), \dot{y}(t), \ddot{y}(t), \dots, y^{(n)}(t)) + d(t)$ or simply f represents the unknown, nonlinear, and variant in the time dynamics of the system. The only information required of the system is its order and the parameter b_0 . The principle in the ADRC has supported consists of the estimation and later cancellation of f . Assuming that f is derivable, the (10) of the system can be represented in (11) as an extended state form [6], [10], [33], [34], [35], [36], [37], [38], [39], [40], [41].

$$\begin{aligned} \dot{x}_1 &= x_2 \\ \dot{x}_2 &= x_3 + bu \\ \dot{x}_3 &= f \\ y &= x_1 \end{aligned} \quad (11)$$

The Linear Extended State Observer (LESO) of (11) will estimate the vector $x = [x_1 \ x_2 \ x_3]^T = [y \ \dot{y} \ f]^T$ which will be characterized by (12)

$$\begin{aligned} \hat{\dot{x}}_1 &= \hat{x}_2 + l_{11}(y - \hat{x}_1) \\ \hat{\dot{x}}_2 &= \hat{x}_3 + l_{21}(y - \hat{x}_1) + bu \\ \hat{\dot{x}}_3 &= l_{31}(y - \hat{x}_1) \end{aligned} \quad (12)$$

The observer gains are calculated as l_{11} , l_{21} , and l_{31} . The observer gains are calculated, so the characteristic polynomial is strictly Hurwitz. For practical reasons, all the LESO poles are in $-w_o$, which is stated (13)

$$s^3 + l_{11}s^2 + l_{21}s + l_{31} = (s + w_o)^3 \quad (13)$$

Generally, higher observer gains represent more exactitude in the estimate. But it must be considered that high gains also increase the sensibility to the measurement noise. The ADRC will cancel the effect of f using \hat{x}_3 through the control law (14) as

$$u = \frac{k_p (r - \hat{x}_1) - k_d \hat{x}_2 - \hat{x}_3}{b_0} \quad (14)$$

Where r is the reference signal, k_d and k_p are the control gains, elected so that the polynomial $s^2 + k_d s + k_p$ be Hurwitz, where w_c is the closed-loop bandwidth that originates in (15).

$$s^2 + k_d s + k_p = (s + w_c)^2 \quad (15)$$

The relationship between the bandwidth observer w_o and the controller w_c the heuristic relationship (16) is used.

$$w_o = (3 \text{ to } 5)w_c \quad (16)$$

When substituting (14) in (10), the system to loop closed transforms in (17).

$$\ddot{y} = (f - \hat{x}_3) + k_p (r - y) - k_d \dot{y} \quad (17)$$

It can be appreciated that the first term to the right of (17) is insignificant, which is the reason that makes the ADRC able to compensate for the effect of f in real-time. To control the process with the ADRC, it is estimated the value of b_0 . With the input signal ($u(t)$) and the output signal ($y(t)$) are reconstructed, in the observer, the output (\hat{x}_1), the state (\hat{x}_2) and the total uncertainty (\hat{x}_3) which includes the external disturbances $d(x, t)$, the modeling imprecision and the uncertain nonlinear dynamics of the process. The controller uses the reconstructed variables; the control loop structure is shown in Fig. 3.

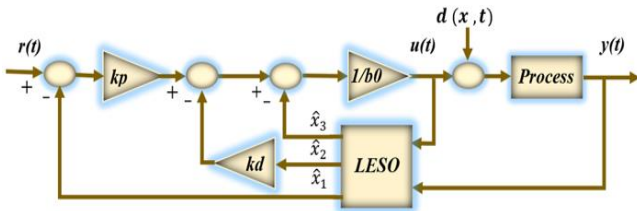


Fig. 3. Process control with the ADRC.

Active Disturbance Rejection Control (ADRC) is a method that does not require a detailed mathematical description of the system [42]. The only information required of the system is its order and the parameter b_0 [43], [44], which are some of its main advantages. Some ADRC consider the plant transfer function coefficients, like the authors of [45], [46], and [47]. In our study, it is proposed to consider only the friction torque described in (4) because it has a non-linear characteristic, which causes difficulties in carrying out the control, causing noise in the links and the position measurements. and speeds.

In (4), the Coulomb and viscosity frictions have been considered to model the friction torque $f_1(\dot{q})$ and $f_2(\dot{q})$, for link 1 as $f_{t1} = f_1(\dot{q})/M_{11}$ and link 2 as $f_{t2} = f_2(\dot{q})/M_{22}$, in a general way f_t the LESO one would be as (18). The control law is in (19).

$$\begin{aligned} \hat{x}_1 &= \hat{x}_2 + l_{11}(y - \hat{x}_1) \\ \hat{x}_2 &= \hat{x}_3 + l_{21}(y - \hat{x}_1) - f_t + bu \\ \hat{x}_3 &= l_{31}(y - \hat{x}_1) \end{aligned} \quad (18)$$

$$u = \frac{k_p (r - \hat{x}_1) - k_d \hat{x}_2 + f_t - \hat{x}_3}{b_0} \quad (19)$$

Proportional Integral Derivative controllers control most industrial robot manipulators. The wide use of robot manipulators in everyday applications is an important reason to study the behavior of Active Disturbance Rejection Control of the robot models with two degrees of freedom.

IV. CONTROL SIMULATION DIAGRAMS AND TRAJECTORIES PLANNING

This section aims to show the general diagrams of the robot model with the ADRC and PID for the uncertainties model, noise, and disturbance in control input of link 2. Also, trajectory planning is explained.

A. Simulation Diagrams

Considering the values of the physical parameters of our robot arm, we obtain the following entries for the robot dynamics in (20)-(23) [17], [18].

$$M(\mathbf{q}) = \begin{bmatrix} 2.351 + 0.168 \cos(q_2) & 0.102 + 0.084 \cos(q_2) \\ 0.102 + 0.084 \cos(q_2) & 0.102 \end{bmatrix} \quad (20)$$

$$C(\mathbf{q}, \dot{\mathbf{q}}) = \begin{bmatrix} -0.168 \sin(q_2) \dot{q}_2 & -0.084 \sin(q_2) \dot{q}_2 \\ 0.084 \sin(q_2) \dot{q}_1 & 0.0 \end{bmatrix} \quad (21)$$

$$g(\mathbf{q}) = g \begin{bmatrix} 3.921 \sin(q_1) + 0.186 \sin(q_1 + q_2) \\ 0.186 \sin(q_1 + q_2) \end{bmatrix} \quad (22)$$

$$f(\dot{\mathbf{q}}) = \begin{bmatrix} 2.288 \dot{q}_1 + f_{c1} \text{sgn}(\dot{q}_1) \\ 0.175 \dot{q}_2 + 1.734 \text{sgn}(\dot{q}_2) \end{bmatrix} \quad (23)$$

The control algorithm against which all controllers are measured is the Proportional-Derivative (PD) controller. We label the torque control action by τ_{pd} . The control law is given by (24) [18] as

$$\tau_{pd} = k_p \tilde{q} + k_d \dot{\tilde{q}} + g(q) + f(\dot{q}) \quad (24)$$

The joint position and velocity errors are denoted by $\tilde{q} = q_d - q$ and $\dot{\tilde{q}} = \dot{q}_d - \dot{q}$.

B. Trajectory Planning

A high level of sustained interest in this field is invariably due to the coupling of inherent constraints and restrictions, the wide-ranging capabilities of robots, the abundance of real-world applications, and the array of possibilities of mechanical systems [23]. Different joint angles will be tested, and a circular trajectory will be tested. The root means square error (E_{RMS}) of the angles of the links will be determined by (25) [11], [33], [48], [49], [50] as

$$E_{RMS} = \sqrt{\frac{\sum_{i=1}^n (\hat{q}_i - q_i)^2}{n}} \quad (25)$$

Where \hat{q} it's a vector of n measurements, q it's the reference vector values, and $i = 1, 2, n$. A fact must be considered for circular trajectory: A Curvature Projection Error (CPE) is introduced to depict the path quality through shape projection. Assume that a good point on how the end effector

performs is given by the following Cartesian coordinates $P = (P_x, P_y)$. The point on the reference path, nearest to point P and part of the equivalent group, is given by: $P_{ref} = (P_{xref}, P_{yref})$. The CPE graph shows the minimal distances between points P and P_{ref} for all samples of the actual path (26) [30], [33], [38], [51].

$$CPE = \sqrt{(P_x - P_{xref})^2 + (P_y - P_{yref})^2} \quad (26)$$

The root means square error (CPE_{RMS}) is computed by (27) [33].

$$CPE_{RMS} = \sqrt{\frac{1}{n} \sum_{i=1}^n CPE^2} \quad (27)$$

The L_2 norm is a widely used tool by the scientific community in robotics to measure control performance. This L_2 norm measures performance control through the root-mean-square of the position error vector. It is given by (28) [17] as

$$L_2 = \sqrt{\frac{1}{T} \int_0^T \frac{1}{T} \|\ddot{q}(\sigma)\| d\sigma} \quad (28)$$

where $T \in \mathbb{R}_+$ represents the simulation time. The Effort index control signal is used, EU , defined as (29) [52], [53] as

$$EU = \int_{t_0}^{t_f} \left| \frac{du(\sigma)}{d\sigma} \right| d\sigma \quad (29)$$

The maximum torques applied by each servomotor of the robot manipulator: $\tau_{1Max} = 135Nm$ and $\tau_{2Max} = 13.5Nm$; for shoulder (first joint) and elbow (second joint), respectively.

V. SIMULATION RESULTS

The objective of this section is to compare the performance of controllers, ADRCs, and PID, controlling the robot. Firstly, the tracking of different link angles was tested, and, finally, a circular trajectory. The control gains used are displayed in Table 1. The gain values of the PID controllers were used by [17], [18], [54].

TABLE 1. THE LINKS POSITIONS

Controller	Parameter
PID link 1	$K_d=150, K_p=2000, K_i=0$
PID link 2	$K_d=15, K_p=1000, K_i=0$
ADRC and ADRC + FC, link 1	$b_{01}=1/(2.351+0.168 \cos(q_2))$ $k_{d1}=50.40, k_{p1}=635.04,$ $l_{11}=378, l_{12}=47628,$ $l_{13}=2000376$
ADRC and ADRC + FC, link 2	$b_{02}=9.9010$ $k_{d2}=75.80, k_{p2}=1436.40,$ $l_{21}=568.5, l_{22}=1.0773 \times 10^5,$ $l_{23}=6.8050 \times 10^6$

A. The Simulation Results for Reference Angles

First, it compared the performance of the controller's ADRCs and PID in tracking different reference angles (see Table 2). Fig. 4(a) shows the behavior of the reference signal

and the fundamental outputs of link 1. Fig. 4(b) shows the behavior of the reference signal and the fundamental outputs of link 2. The error in the output signal of links 1 and 2 with ADRCs is lower than with the PID, as shown in Fig. 4(c) and 4(d), respectively. The links controlled with the ADRC+FC have less noise.

TABLE 2. THE LINKS POSITIONS

Link	Position 1 (degree)	Position 2 (degree)
Link 1	45	60
Link 2	90	-30

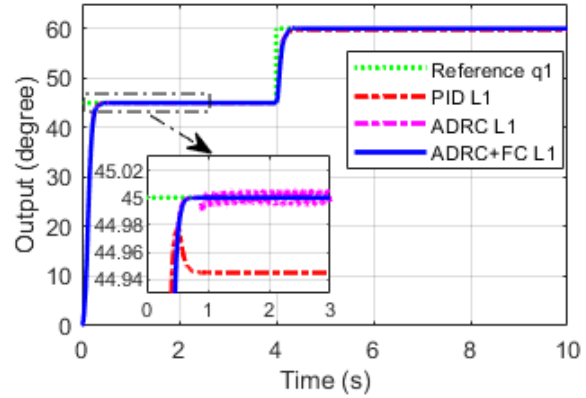


Fig. 4(a). Performance of ADRCs and PID controllers. Reference and outputs, link 1

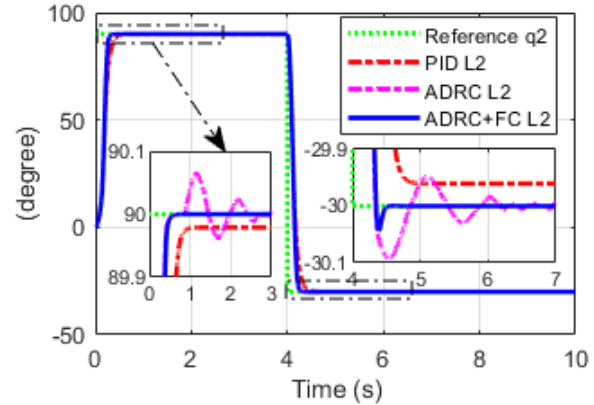


Fig. 4(b). Performance of ADRCs and PID controllers. Reference and outputs, link 2.

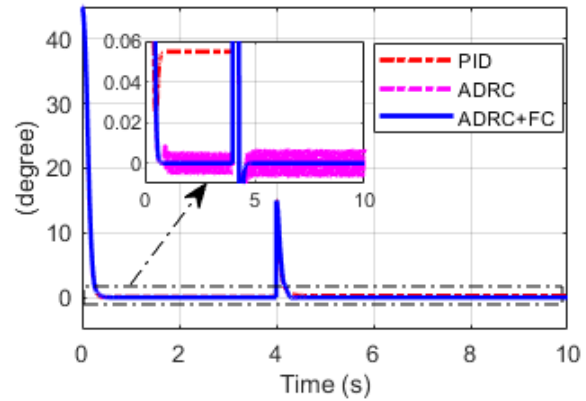


Fig. 4(c). Error PID and ADRCs, link 1.

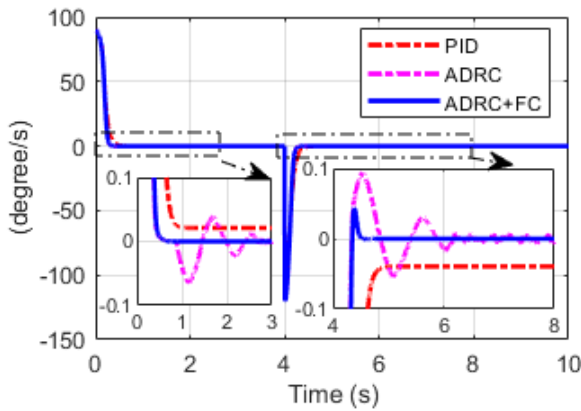


Fig. 4(d). Error PID and ADRCs, link 2.

Shown in Fig. 5(a) are the controller outputs of the link 1 controllers. Fig. 5(b) the controller outputs of link 2. Fig. 5(c) the effort of the link 1 controllers. 5(d) link 2 controller effort. The ADRCs perform less effort than PID.

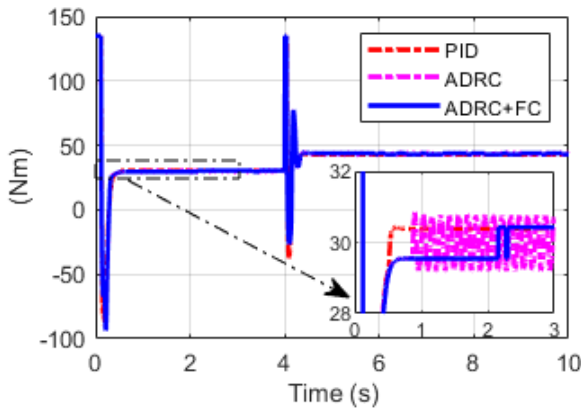


Fig. 5(a). Controller outputs, link 1.

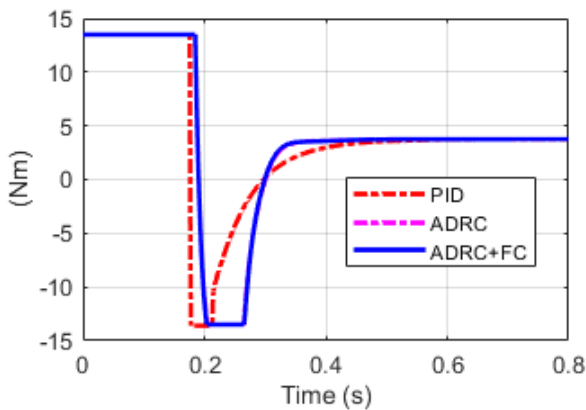


Fig. 5(b). Controller outputs, link 2.

Table 3 shows that the median and interquartile values for links 1 and 2 are smaller for the ADRCs than for the PID. The noise and variations in the output of the ADRC+FC are smaller than with the ADRC. Fig. 6 shows the L_2 norm of the controllers' evaluation. The L_2 norm of the ADRCs is smaller than those of the PID.

The root means square error (E_{RMS}) box-and-whisker plot [55] for the vector of position using PID and ADRC controllers is observed in Fig. 7. The bottom for the PID is

0.0237 degrees, and ADRCs are 0.0 degrees, the top for the PID value is 0.1343 degrees, the top for the ADRC is 4.3626×10^{-5} degrees, and the top for the ADRC+FC is 2.2284×10^{-11} degrees; the median and the values of the quartiles are displayed in Table 3. It is appreciated that the variability with the ADRC+FC is smaller than with the ADRC and PID because its box has a smaller size, and a minor interquartile difference exists.

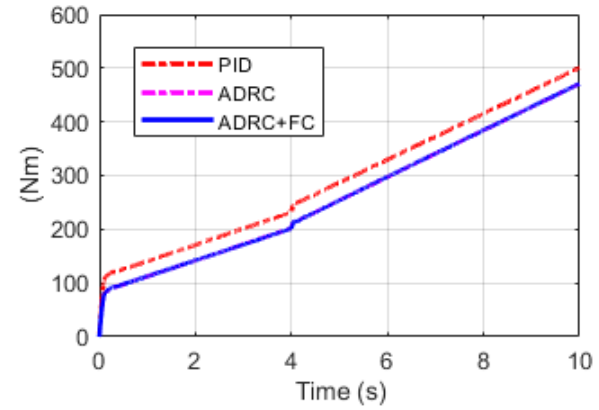


Fig. 5(c). The controllers' effort, link 1.

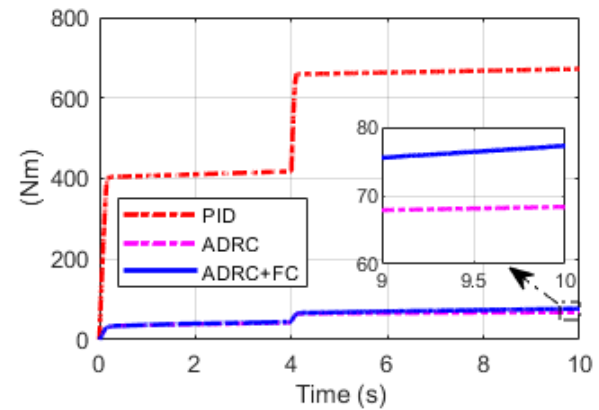


Fig. 5(d). The controllers' effort, link 2.

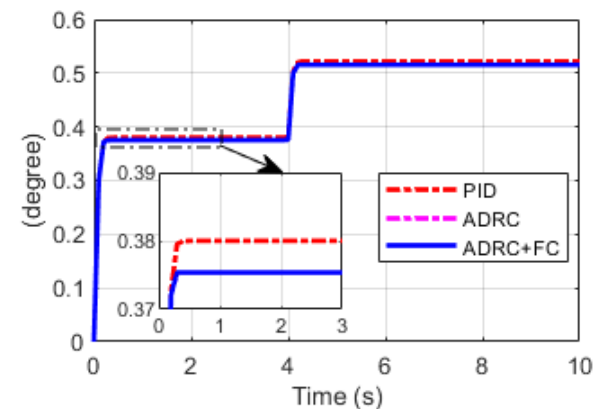


Fig. 6. The L_2 norm for PID and ADRCs.

TABLE 3. THE CONTROLLERS' PID AND ADRC RESULTS

Controller	1° Quartile (degree)	Median (degree)	3° Quartile (degree)
PID	0.0451	0.0742	0.1222
ADRC	4.7903×10^{-6}	8.5557×10^{-6}	2.0330×10^{-5}
ADRC+FC	6.4415×10^{-17}	1.8219×10^{-16}	9.0440×10^{-12}

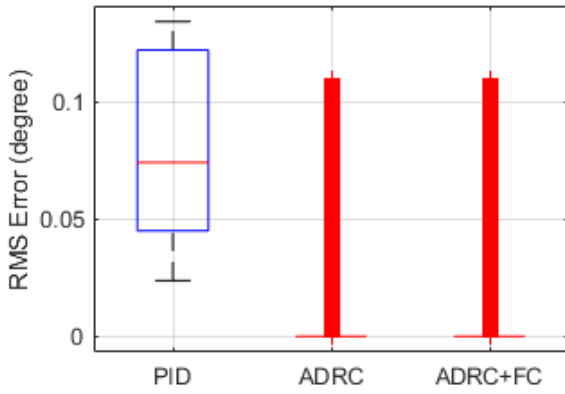


Fig. 7. The root means square error (E_{RMS}) box-and-whisker plot using PID and ADRCs controllers.

B. The Velocity Estimate with the ADRC

Fig. 8(a) plots the difference between the real and the estimated velocities of link 1, and the zoom shows that such difference is smaller than 1.5 degree/s; for ADRC. Fig. 8(b) plots the difference between the real and the estimated velocities of link 2, and the zoom shows that such difference is smaller than 1% (7 degree/s). Fig. 8(c) plots the difference between the real and the estimated velocities of link 1, and the zoom shows that such difference is smaller than 1.5 degree/s; for ADRC+FC. Fig. 8(d) plots the difference between the real and the estimated velocities of link 2, and the zoom shows that such difference is smaller than 1% (5 degree/s). Fig. 8(e) shows a plot of the error in link 1. Fig. 8 (f) shows a plot of the error in link 2.

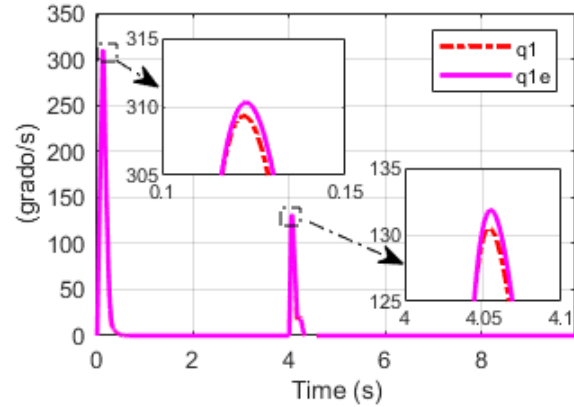


Fig. 8(c). The real velocity and the estimated one, link 1, ADRC+FC.

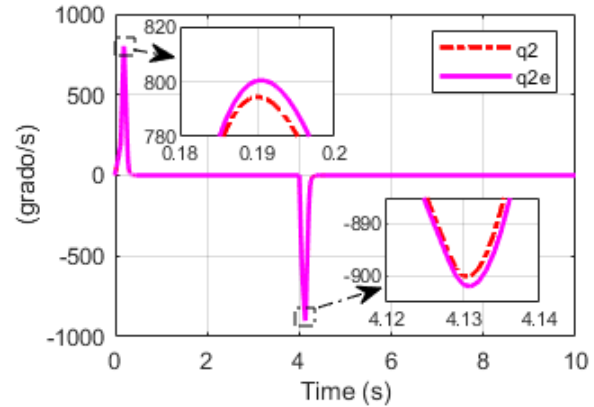


Fig. 8(d). The real velocity and the estimated one, link 2, ADRC+FC.

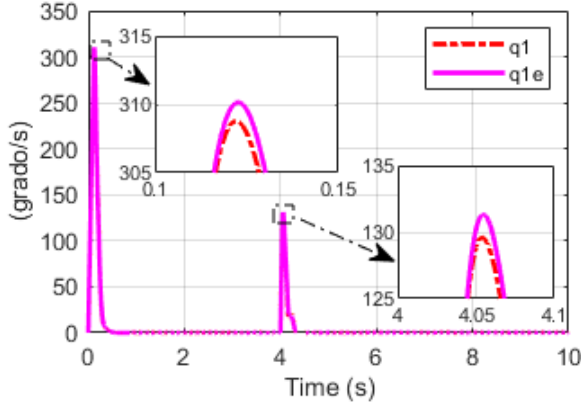


Fig. 8(a). The real velocity and the estimated one, link 1, ADRC.

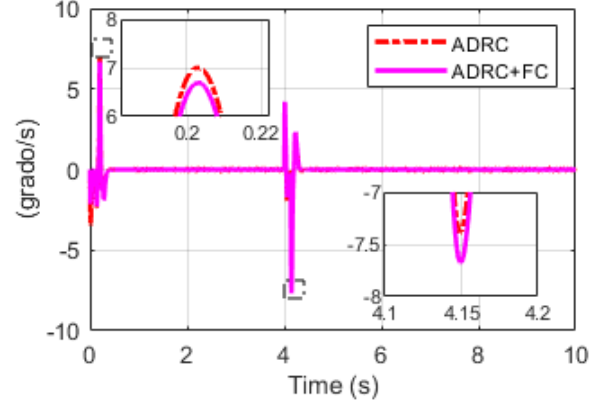


Fig. 8(e). Error velocities ADRC and ADRC+FC, link 1.

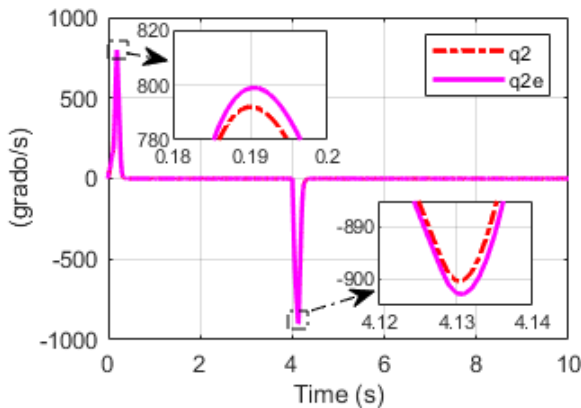


Fig. 8(b). The real velocity and the estimated one, link 2, ADRC.

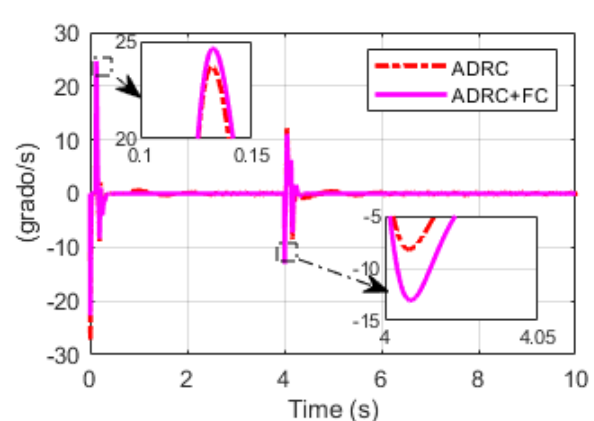


Fig. 8(f). Error velocities ADRC and ADRC+FC, link 2.

C. The Simulation Results for Circular Reference

The second experiment compares the robot model with ADRC, ADRC+FC, and PID controllers, both following a circular reference with origin on the $x - y$ axis (0.0; 0.05) m and a radius of 0.8 m.

In Fig. 9, the reference and real trajectories of link 2. Fig. 10 is the L_2 norm for PID and ADRCs and is smaller for PID than those of the ADRCs. Fig. 11 displays the trajectory RMS error (CPE_{RMS}) in the box plot. The bottom for the PID and ADRCs is 0.0 m; meanwhile, the top for the PID is 2.3775×10^{-4} m, and for the ADRCs is 1.4752×10^{-4} m. The median and the values of the quartiles are shown in Table 4.

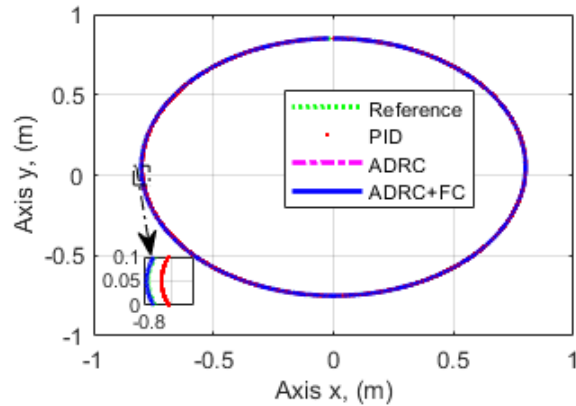


Fig. 9. Trajectories link 2.

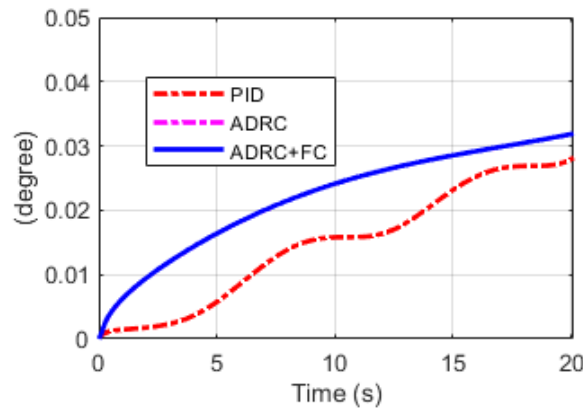


Fig. 10. The L_2 norm for PID and ADRCs.

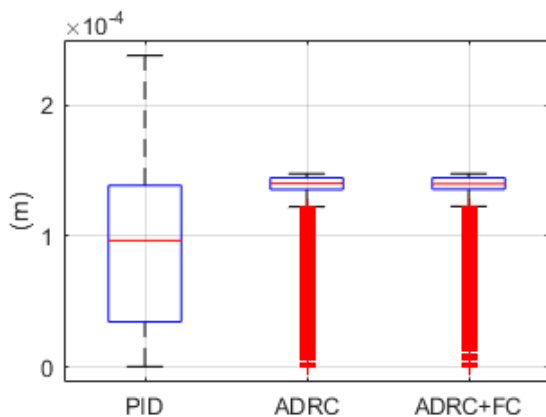


Fig. 11. The root means square error (CPE_{RMS}) box-and-whisker plot using PID and ADRCs controllers.

TABLE 4. THE CONTROLLERS' RMS RESULTS FOR CIRCULAR TRAJECTORY

Controller	1° Quartile (m)	Median (m)	3° Quartile (m)
PID	3.4467×10^{-05}	9.6512×10^{-05}	1.3858×10^{-04}
ADRC	1.3551×10^{-04}	1.4018×10^{-04}	1.4449×10^{-04}
ADRC+FC	1.3569×10^{-04}	1.3985×10^{-04}	1.4449×10^{-04}

D. The Velocity Estimate with the ADRC

Fig. 12(a) shows the difference between the real and the estimated velocities of link 1, and the zoom indicates that such a difference is smaller than 0.1 deg/s for ADRC. Fig. 12(b) shows the difference between the real and the estimated velocities of link 2, and the zoom shows that such a difference is smaller than 0.1 degree/s for a stable state. Fig. 12(c) plots the difference between the real and the estimated velocities of link 1, and the zoom shows that such difference is smaller than 0.1 degree/s; for ADRC+FC. Fig. 12(d) plots the difference between the real and the estimated velocities of link 2, and the zoom shows that such a difference is smaller than 0.1 degree/s. Fig. 12(e) shows a plot of the error in link 1, and Fig. 12(f) shows a plot of the error in link 2. The noise and the variations in the output of the ADRC+FC are smaller than with the ADRC.

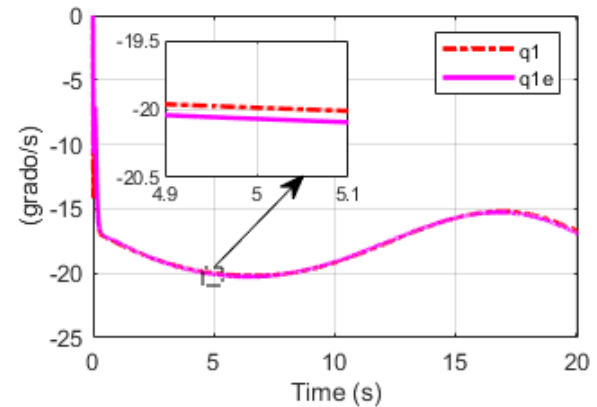


Fig. 12(a). Velocities real and estimate of link 1, ADRC.

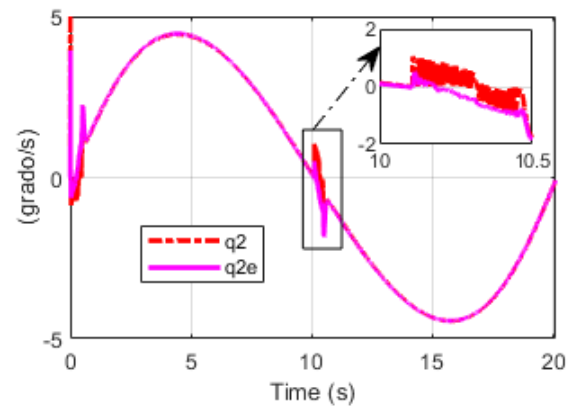


Fig. 12(b). Velocities real and estimate of link 2, ADRC.

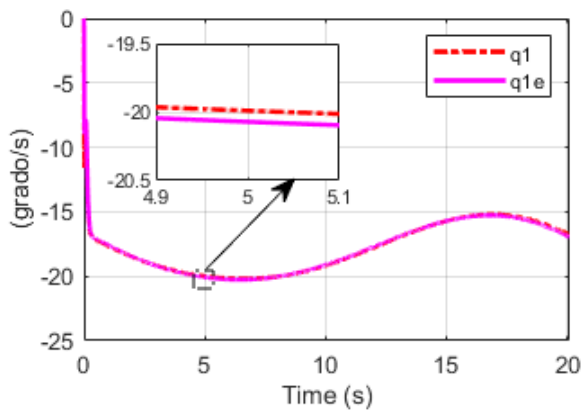


Fig. 12(c). Velocities real and estimate of link 1, ADRC+FC.

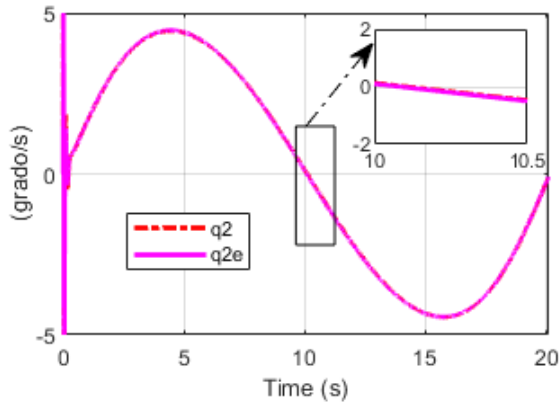


Fig. 12(d). Velocities real and estimate of link 2, ADRC+FC.

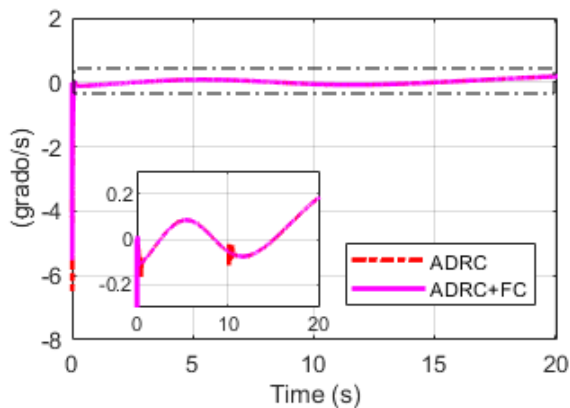


Fig. 12(e). Error velocities ADRCs, link 1.

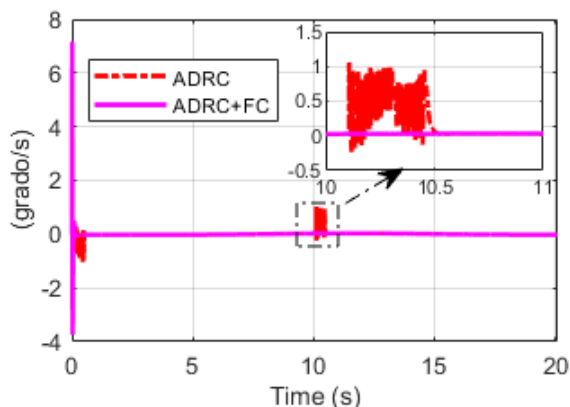


Fig. 12(f). Error velocities ADRCs, link 2.

CONCLUSION

This paper compared the ADRC, the ADRC+FC, an ADRC with torque friction compensation, and the PID controllers for the two degrees of freedom robot model. The root means square errors for different angles of links are smaller than 0.1343 degrees, and this error is smaller with the ADRC+FC than with the ADRC and PID controllers. The ADRC and the ADRC+FC estimate the link velocities with an error smaller than 1%, although that of ADRC+FC is smaller. The controllers meet the requirements, but in reference angle tracking, the ADRC+FC is better; in circular path tracking, the PID performance is better. ADRCs estimate link speeds internally, making mechanical measuring devices unnecessary.

REFERENCES

- [1] J. Gong, W. Wei, G. Cai, Y. Liu, and X. Peng, "Kinematic Performance Analysis of a Controllable Mechanism Welding Robot with Joint Clearance," *MATEC Web of Conferences*, vol. 327, pp. 03006, 2020, doi: 10.1051/mateconf/202032703006.
- [2] B. Altiner, A. Delibasxi, and B. Erol, "Modeling and control of flexible link manipulators for unmodeled dynamics effect. *Journal Systems and Control Engineering*," *Proceedings of the Institution of Mechanical Engineers, Part I: Journal of Systems and Control Engineering*, vol. 233, pp. 245-263, 2019, doi: 10.1177/0959651818791071.
- [3] A. AlAttar and P. Kormushev, "Kinematic-Model-Free Orientation Control for Robot Manipulation Using Locally Weighted Dual Quaternions," *Robotics*, vol. 9, pp. 76, 2020, doi: 10.3390/robotics9040076.
- [4] K. Pasha, "A suggested simple design and inverse kinematics for a multi-degrees-of-freedom robot arm," *International Robotics & Automation Journal*, vol. 7, pp. 103-110, 2021, doi: 10.15406/iratj.2021.07.00234.
- [5] B. Chen and J. Huang, "Decreasing infinite-mode vibrations in single-link flexible manipulators by a continuous function," *Proceedings of the Institution of Mechanical Engineers, Part I: Journal of Systems and Control Engineering*, vol. 231, pp. 436-446, 2017, doi: 10.1177/0959651817708489.
- [6] X. Cheng, X. Tu, Y. Zhou, and R. Zhou, "Active Disturbance Rejection Control of Multi-Joint Industrial Robots Based on Dynamic Feedforward," *Electronics*, vol. 8, pp. 591, 2019, doi: 10.3390/electronics8050591.
- [7] A. J. Humaidi, H. M. Badr, and A. R. Ajil, "Design of Active Disturbance Rejection Control for Single-Link Flexible Joint Robot Manipulator," *2018 22nd International Conference on System Theory, Control and Computing (ICSTCC)*, pp. 452-457, 2018, doi: 10.1109/ICSTCC.2018.8540652.
- [8] X. Wenchao, R. Madoński, K. Łakomy, and Z. Gao, "Add-On Module of Active Disturbance Rejection for Set-Point Tracking of Motion Control Systems," *IEEE Transactions on Industry Applications*, vol. 53, pp. 4028-4040, 2017, doi: 10.1109/TIA.2017.2677360.
- [9] J. Han, "From PID to Active Disturbance Rejection Control," *IEEE Transactions on Industrial Electronics*, vol. 56, pp. 900-906, 2019, doi: 10.1109/TIE.2008.2011621.
- [10] G. Zhiqiang, "Active disturbance rejection control: a paradigm shift in feedback control system design," *2006 American Control Conference*, vol. 7, 2006, doi: 10.1109/ACC.2006.1656579.
- [11] R. Fareh, M. Al-Shabi, M. Bettayeb, and J. Ghommam, "Robust Active Disturbance Rejection Control for Flexible Link Manipulator," *Robotica*, vol. 38, no. 1, pp. 1-18, 2019, doi: 10.1017/S026357471900050X.
- [12] Y. Huang, W. Xue, G. Zhiqiang, H. Sira-Ramirez, D. Wu, and M. Sun, "Active disturbance rejection control: Methodology, practice and analysis," *Proceedings of the 33rd Chinese Control Conference*, pp. 1-5, 2014, doi: 10.1109/ChiCC.2014.6896585.
- [13] L. Sun, J. Dong, and K. Lee, "A Practical Multivariable Control Approach Based on Inverted Decoupling and Decentralized Active

- Disturbance Rejection Control,” American Chemical Society, vol. 55, no. 7, pp. 2008-2019, 2016, doi: 10.1021/acs.iecr.5b03738.
- [14] C. Wang, J. Huang, C. Wang, and R. Wu, “Dynamic Surface-Active Disturbance Rejection Control for Two-Wheeled Self-Balancing Robot,” *ICRCA '18: Proceedings of the 3rd International Conference on Robotics, Control and Automation*, pp. 82–87, 2018, doi: 10.1145/3265639.3265645.
- [15] H. Coral-Enriquez and S. Pulido-Guerrero, “Sway reduction in tower-cranes through discrete-time resonant active disturbance rejection control,” 2017, vol. 85, pp. 65-75, 2017, DOI: doi: 10.15446/dyna.v85n204.63245.
- [16] Z. Zhou, S. B. Elghali, M. Benbouzid, Y. Amirat, E. Elbouchikhi, and G. Feld, “Tidal stream turbine control: An active disturbance rejection control approach,” *Ocean Engineering*, vol. 202, pp. 107190, 2020, doi: 10.1016/j.oceaneng.2020.107190.
- [17] B. Sánchez-García, F. Reyes-Cortés, B. M. Al-Hadithi, and Olga Félix-Beltrán “Global Saturated Regulator with Variable Gains for Robot Manipulators”, *Journal of Robotics and Control (JRC)*, vol. 2, no. 6, pp 571-581, 2021, doi: 10.18196/jrc.26139.
- [18] F. Reyes and R. Kelly, “Experimental evaluation of model-based controllers on a direct-drive robot arm”, *Mechatronics*, vol. 11, pp 267-282, 2001, doi: 10.1016/S0957-4158(00)00008-8.
- [19] R. Kelly, V. Santibañez Davila, and A. Loria, *Control of Robot Manipulators in Joint Space*, 2005 ed. Springer, London, 2005.
- [20] T. S. Lee, E. A. Alandoli, and V. Vijayakumar, “2-DOF robot modelling by SimMechanics and PD-FL integrated controller for position control and trajectory tracking,” *F1000Research*, vol. 10, pp. 1045, 2021, doi: 10.12688/f1000research.72912.2.
- [21] F. J. Torres, G. V. Guerrero, C. D. García, J. F. Gomez, M. Adam, and R. F. Escobar, “Master-Slave Synchronization of Robot Manipulators Driven by Induction Motors,” *IEEE Latin America Transactions*, vol. 14, pp. 3986-3991, 2016, doi: 10.1109/TLA.2016.7785923.
- [22] N. M. Ghaleb, and A. Ayman, “Modeling and Control of 2-DOF Robot Arm,” *International Journal of Emerging Engineering Research and Technology*, vol. 6, no. 11, pp. 24-31, 2018.
- [23] C. S. Jeong, J. S. Kim, and S. I. Han, “Tracking Error Constrained Super-twisting Sliding Mode Control for Robotic Systems,” *Int. J. Control Autom. Syst.*, vol. 16, pp. 804–814, 2018, doi: 10.1007/s12555-017-0134-y.
- [24] M. Baccouch and S. A. Dodds, “Two-Link Robot Manipulator: Simulation and Control Design,” *International Journal of Robotic Engineering*, vol. 5, pp. 2-17, 2020, doi: 10.35840/2631-5106/4128.
- [25] H. Hussein Mohammed Al-Almoodi, N. Zainul Azlan, I. Shahdad, and N. Kamaruzaman “Continuous Passive Motion Machine for Elbow Rehabilitation,” *International Journal of Robotics and Control Systems*, vol. 1, no. 3, pp 402-415, 2021, doi: 10.31763/ijres.v1i3.446 .
- [26] F. G. Salas, J. Orrante-Sakanassi, R. Juarez-del-Toro, and R. P Parada, “A stable proportional–proportional integral tracking controller with self-organizing fuzzy-tuned gains for parallel robots,” *International Journal of Advanced Robotic Systems*, vol. 16, no. 1, pp 1–16, 2019, doi: 10.1177/1729881418819956.
- [27] P. Corke, *Robotics, Vision and Control*, 2nd Edition, Springer International Publishing AG, 2017.
- [28] G. Goodwin, S. Graebe, and M. Salgado, *Control System Design*, Pearson Education, 2001.
- [29] K. Ogata, *Ingeniería de Control Moderna*. Pearson Education, S.A, Inc. 2010, 5th Edition.
- [30] A. O’Dwyer, *Handbook of PI and PID Controller Tuning Rules*, Imperial College Press, 2009. 3rd Edition.
- [31] R. Beltrán Aguedo, A. Lussón Cervantes, J. R. Nuñez Alvarez, and Y. Llosas Albuérne, “Speed control in DC and AC drives,” *International Journal of Power Electronics and Drive Systems (IJPEDS)*, vol. 14, pp. 2006-2017, 2021, doi: 10.11591/ijpeds.v12.i4.pp2006-2017.
- [32] D. Xue, Y. Chen, and D. Atherton, *Linear Feedback Control Analysis and Design with MatLab*, Society for Industrial and Applied Mathematics, 1st Edition, 2007, pp. 370.
- [33] M. Przybyła, M. Kordasz, R. Madoński, P. Herman, and P. Sauer, “Active Disturbance Rejection Control of a 2DOF manipulator with significant modeling uncertainty,” *Bulletin of The Polish Academy of Sciences-technical Sciences*, vol. 60, pp. 509-520, 2012, doi: 10.2478/v10175-012-0064-z.
- [34] D. Milanés-Hermosilla, R. Trujillo Codorniu, R. López-Baracaldo, R. Sagaró-Zamora, D. Delisle-Rodríguez, J. J. Villarejo-Mayor, and J. R. Núñez-Álvarez, “Monte Carlo Dropout for Uncertainty Estimation and Motor Imagery Classification,” *Sensors*, vol. 21, pp. 7241, 2021, doi: 10.3390/s21217241.
- [35] A. Prasad, B.;Sharma, and J Vanualailai, “A new stabilizing solution for motion planning and control of multiple robots,” *Robotica*, vol. 34, pp. 1071-1089, 2014, doi: 10.1017/S0263574714002070.
- [36] W. Qing L. Tao N. Zhuo H. Shoulin R. Xuhui, Z. Dan, and W. Lei, “A generalized control scheme for system uncertainty estimation and cancellation,” *Automation in Mechatronic and Robotic Systems*, vol. 43, pp. 2921-2933, 2021, doi: 10.1177/01423312211010509.
- [37] G. Li, L. Pan, Q. Hua, L. Sun, and K. Y. Lee, “Water Pump Control: A Hybrid Data-Driven and Model-Assisted Active Disturbance Rejection Approach,” *Water*, vol. 11, pp. 1066, 2019, doi: 10.3390/w11051066.
- [38] Y. Fan, J. Shao, G. Sun, and X. Sha, “Active Disturbance Rejection Control Design Using the Optimization Algorithm for a Hydraulic Quadruped Robot,” *Computational Intelligence and Neuroscience*, vol. 2021, pp. 1-22, 2021, doi: 10.1155/2021/6683584.
- [39] D. Milanés Hermosilla, R. Trujillo Codorniu, R. Lopez Baracaldo, R. Sagaró Zamora, D. Delisle Rodríguez, Y. Llosas Albuérne, and J. R. N. Alvarez, “Shallow Convolutional Network Excel for Classifying Motor Imagery EEG in BCI Applications,” *IEEE Access*, vol. 9, pp. 98275–98286, 2021, doi: 10.1109/ACCESS.2021.3091399.
- [40] M. Stankovic, R. Madonski, S. Shao, and D. Miklu, “On dealing with harmonic uncertainties in the class of active disturbance rejection controllers,” *International Journal of Control*, vol. 94, pp. 2795-2810, 2020, doi: 10.1080/00207179.2020.1736639.
- [41] X. Zhou, Y. Cui, and Y. Ma, “Fuzzy Linear Active Disturbance Rejection Control of Injection Hybrid Active Power Filter for Medium and High Voltage Distribution Network,” *IEEE Access*, vol. 9, pp. 8421-8432, 2021, doi: 10.1109/ACCESS.2021.3049832.
- [42] P. Teppa-Garran and G. García, “Optimal Tuning of PI/PID/PID Controllers in Active Disturbance Rejection Control,” *Control Engineering and Applied Informatics*, vol. 15, pp 26-36, 2013.
- [43] Z. Gao, “Scaling and Bandwidth-Parameterization Based Controller Tuning,” *Proceedings of the 2003 American Control Conference*, 2003, pp. 4989-4996, doi: 10.1109/ACC.2003.1242516.
- [44] G. Herbst, “A Simulative Study on Active Disturbance Rejection Control (ADRC) as a Control Tool for Practitioners,” *Electronics*, vol. 2, pp. 246–279, 2013.
- [45] S. Zhao, L. Sun, D. Li and Z. Gao, “Tracking and Disturbance Rejection in Non-minimum Phase Systems,” *Proceedings of the 33rd Chinese Control Conference*, 2014, pp. 3834-3839, doi: 10.1109/ChiCC.2014.6895578.
- [46] L. Sun, D. Li, Z. Gao, Z. Yang, and S. Zhao, “Combined feedforward and model-assisted active disturbance rejection control for non-minimum phase system”, *ISA Transactions*, vol. 64, pp 24-33, 2016, doi: 10.1016/j.isatra.2016.04.020.
- [47] L. Sun, G. Li, Q.S. Hua, and Y. Jin, “A hybrid paradigm combining model-based and data-driven methods for fuel cell stack cooling control,” *Renewable Energy*, vol. 174, Part 1, pp 1642-1652, 2019, doi: 10.1016/j.renene.2019.09.048.
- [48] G. Yu. M. Kulikov, and V. Kulikova, “Overall hyperbolic-singular-value-decomposition-based square-root solutions in Kalman filters with deterministically sampled mean and covariance for state estimation in continuous-discrete nonlinear stochastic systems,” *European Journal of Control*, vol. 66, pp. 100648, 2022, doi: 10.1016/j.ejcon.2022.100648.
- [49] S. D. Perkasa, P. Megantoro, and H. A. Winarno, “Implementation of a Camera Sensor Pixy 2 CMUcam5 to A Two Wheeled Robot to Follow Colored Object,” *Journal of Robotics and Control (JRC)*, vol. 2, no. 6, pp. 496-501, doi: 10.18196/jrc.26128.
- [50] B. T. AIKhlidi, A. Abdulsadda, and A. Al Bakri, “Optimal Robotic Path Planning Using Intelligents Search Algorithms,” *Journal of Robotics and Control (JRC)*, vol. 2, no. 6, pp. 519-526, 2021, doi: 10.18196/jrc.26132

- [51] K. Gao, J. Song, X. Wang, and H. Li, "Fractional-order proportional-integral-derivative linear active disturbance rejection control design and parameter optimization for hypersonic vehicles with actuator faults," *Tsinghua Science and Technology*, vol. 26, no. 1, pp. 9-23, 2021, doi: 10.26599/TST.2019.9010041.
- [52] K. J. Åström and T. Hägglund, *PID controllers: theory, design, and tuning*, 2nd Edition, 1995.
- [53] I. O. Benitez González, R. Rivas Perez, V. Feliu Batlle, and F. Castillo García, "Temperature Control Based on a Modified Smith Predictor for Injectable Drug Formulations," *IEEE Latin America Transactions*, vol. 13, no. 4, pp. 1041-1047, 2015, doi: 10.1109/TLA.2015.7106355.
- [54] L. Peña-Pupo, H. Martínez-García, E. García-Vílchez, E. Y. Fariñas-Wong, and J. R. Núñez-Álvarez, "Combined Method of Flow-Reduced Dump Load for Frequency Control of an Autonomous Micro-Hydropower in AC Microgrids," *Energies*, vol. 14, no. 23, pp. 8059, 2021, doi: 10.3390/en14238059
- [55] A. W. Shardt, *Statistics for Chemical and Process Engineers*, Springer International, 2015.